Journal of Electroceramics 4:1, 225–231, 2000

Structural, Thermal and Electrical Properties of Ce-Doped $SrMnO_3$

S. HASHIMOTO & H. IWAHARA

Center for Integrated Research in Science and Engineering, Nagoya University, Furo-cho, Chikusa-ku, Nagoya, 464-8603, Japan

Submitted April 2, 1999; Revised May 28, 1999; Accepted August 30, 1999

Abstract. The $Sr_{1-x}Ce_xMnO_{3-\alpha}$ system ($0 \leq x \leq 0.5$) was investigated with respect to its structural, thermal and electrical properties. Although un-doped $SrMnO_3$ has the perovskite structure above 1400°C, the structure is unstable at room temperature. However, partial substitution of Ce for Sr in $SrMnO_3$ stabilizes the perovskite structure down to room temperature. Single phase perovskite is obtained for $0.1 \leq x \leq 0.3$ in $Sr_{1-x}Ce_xMnO_{3-\alpha}$, and it remains stable even following heat treatment at 800°C for 100 h. The dependence of the electrical conductivity on temperature was measured from room temperature to 1000°C in air. Ce doping dramatically enhanced the electrical conductivity of $SrMnO_3$. $Sr_{0.7}Ce_{0.3}MnO_{3-\alpha}$ exhibits a higher conductivity (290 $S \cdot cm^{-1}$ at 1000°C) than that of $La_{0.8}Sr_{0.2}MnO_3$ (LSM, about 175 $S \cdot cm^{-1}$) and remains n-type over the whole range of temperature examined. The thermal expansion coefficients in the system were nearly constant with values ranging between 1.24×10^{-6} and 1.01×10^{-6} cm/cm · K for temperatures of 50°C to 1000°C.

Keywords: Ce-doped $SrMnO_3$, electrical conductivity, perovskite, SOFC cathode, Seebeck coefficient

1. Introduction

Sr-doped $LaMnO_3$ (LSM) is the most commonly used material as the cathode in solid oxide fuel cells (SOFC). However, because lanthanum is difficult to separate from other light rare earth metals, it becomes costly. Although cerium is also a light rare earth metal, separation is rather easy because of its stable tetravalent state.

For cost reduction of the cathode material, it is desirable to use smaller amounts of low cost rare earth metal. Iwahara and Esaka et al. [1] reported that Ce-doped $CaMnO_3$ would be an SOFC cathode material candidate, and that the properties of $Ca_{0.9}Ce_{0.1}MnO_{3-\alpha}$, e.g. conductivity, thermal expansion, catalytic activity and so on, were almost comparable with those of conventional LSM. In this oxide, cerium is partially substituted for Ca, but it has a lower content of rare earth element compared with LSM.

In the case of Ce-doped $CaMnO_3$, the solubility limit of Ce was only 10% in the A-site which is too low to induce enough of a shift in manganese valence. In the present study, we focused on Ce-doped $SrMnO_3$. Assuming a higher substitution of Ce for Sr in Ce-doped $SrMnO_3$, we would expect a higher conductivity leading to possible application of the material as the cathode in an SOFC operating at intermediate temperature. However, un-doped $SrMO_3$ doesn't have the perovskite structure below 1400°C [2] and its conductivity is much lower than that of LSM [8].

In this study, we investigated the stabilization of the perovskite structure in $SrMnO_3$ by partial substitution of cerium for strontium and the conductivity of the resultant solid solution $Sr_{1-x}Ce_xMnO_{3-\alpha}$ ($0 \leq x \leq 0.5$).

2. Experimental

The specimens were prepared from $SrCO_3$ of 99.99% purity, CeO_2 and Mn_2O_3 of 99.9% purity. The powders of the required proportion were mixed and calcined in air at 1100°C for 10 h. The calcined specimens were crushed and ground in a satellite-type ball mill into fine powders for 1 h. The powders were pressed into cylindrical pellets under a hydrostatic pressure of 2 ton/cm^2. The pellets of Ce doped

$SrMnO_3$ were sintered in air at 1400 to 1480°C for 10 h. For un-doped $SrMnO_3$, some pellets were sintered at 1350°C for 30 h and held at 900°C in air to obtain the hexagonal structure, the other pellets were quenched into water after sintering at 1500°C for 10 h to obtain the perovskite structure. The densities of the sintered ceramics of Ce-doped $SrMnO_3$ were over 95% of theoretical while that of non-doped hexagonal $SrMnO_3$ was 92%.

The formation of compounds, the solid solubility of dopant and the lattice parameters ware confirmed by X-ray diffraction using CuKα radiation with a Rigaku Rint 2000. To confirm the thermal stabilities of un-doped $SrMnO_3$ and the Ce doped $SrMnO_3$, the specimens which were annealed in air at 800°C for 100 h were analyzed by X-ray diffraction.

Thermal expansion was measured from room temperature to 1000°C by a thermal mechanical analyzer (TMA) Rigaku CN8098F2, and the the phase transition was investigated up to 1000°C by a differential thermal analyzer (DTA) Rigaku MJ8000KT2.

The electrical conductivity was measured by the dC four-probe method. The voltages were measured under at least four different current values, and the electrical conductivities were calculated from linear *I-V* plots. The Seebeck coefficient was determined by placing specimens under temperature gradients in the furnace, monitoring the temperatures at the both ends of the specimens by K-type thermocouples and measuring the induced voltage across the specimens.

3. Results and Discussion

3.1. Formation of Compounds and Microstructure

Figure 1 shows XRD patterns of un-doped $SrMnO_3$ and $Sr_{1-x}Ce_xMnO_{3-\alpha}$ after slow cooling (3.5–3.2°C/min) from the sintering temperature. Negas and Roth reported that un-doped $SrMnO_3$ has the hexagonal 4L structure below 1035°C and changes into an anion-deficient perovskite-type structure above 1400°C [2]. Un-doped $SrMnO_3$, which had been annealed at 900°C for 10 h after sintering at 1350°C for 30 h, gave XRD patterns of the hexagonal four layered (4L) structure (Fig. 1(a)).

Only 5% substitution of cerium for strontium in $SrMnO_3$ stabilized the perovskite structure down to room temperature and the XRD pattern consisted of

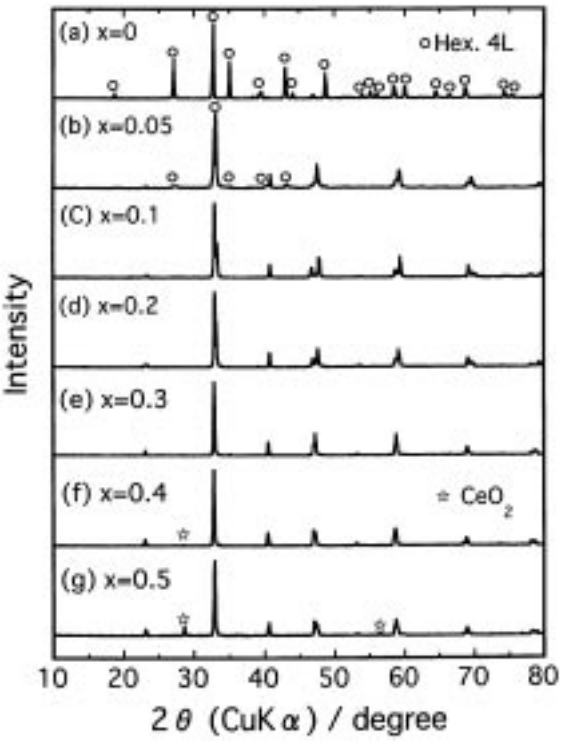

Fig. 1. X-ray diffraction patterns of $Sr_{1-x}Ce_xMnO_{3-a}$ $(x = 0 - 0.5)$.

the diffraction peaks for the hexagonal 4L structure and the perovskite structure (Fig. 1(b)). Figure 2 shows XRD patterns of $Sr_{0.95}Ln_{0.05}MnO_3$ (Ln = Ce, La, Pr or Sm). Each Ln without cerium also had the ability of stabilizing the perovskite structure although it was not so effective as that of cerium. It is known that cerium can take the tetravalent easier than other light rare earth elements. This property of cerium would affect the stabilization of the perovskite structure although the actual valence of cerium was not analyzed clearly because of measurement difficulty in this system.

Single phase perovskite was observed in the composition range from $x = 0.1$ to 0.3 in $Sr_{1-x}Ce_xMnO_{3-\alpha}$ as shown (Fig. 1(c)(d)(e)) and CeO_2 as a second phase was observed in specimens for $x \geq 0.4$ (Fig. 1(f)(g)). The perovskite phase in each $Sr_{1-x}Ce_xMnO_{3-\alpha}$ was tetragonal at room temperature. Figure 3 shows the lattice parameter (*a*,*c*) and unit cell volume *V* which depend on cerium concentration. In the region of single phase perovskite, *a* (*b*-) and *c*-axis became closer to each other as the cerium concentration was increased and the

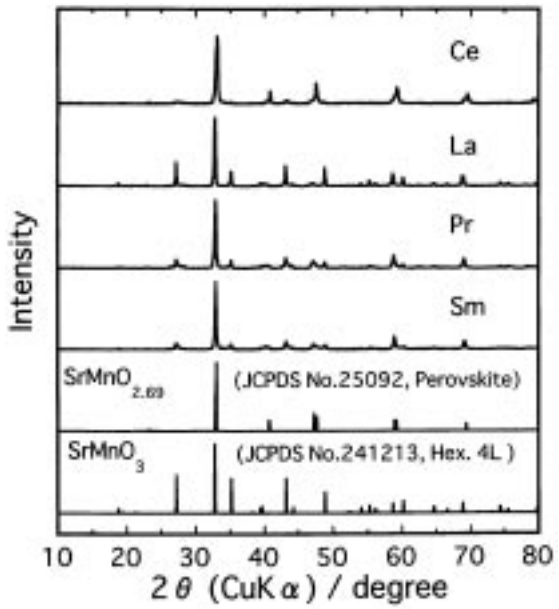

Fig. 2. X-ray diffraction patterns of $Sr_{0.95}Ln_{0.05}MnO_{3-\alpha}$ (Ln = Ce, La, Pr, Sm).

crystalline symmetry became the highest at $x = 0.3$. This dependence of cerium concentration on the lattice parameter doesn't always correspond with the ionic radii of cations in the perovskite lattice. Although Ce^{3+} (1.34 Å at coordination number (CN) 12) and Ce^{4+} (1.14 Å at CN = 12) are smaller than Sr^{2+} (1.44 Å at CN = 12) [5], the unit cell volume V increases with increasing cerium concentration in the range of $0.1 \leq x \leq 0.3$. Generally, in the ABO_3 perovskite, there are some cases where body-centered A-site cations influence the Madelung potential and make the stability of the phase change [6]. In case of $Sr_{0.7}Ce_{0.3}MnO_{3-\alpha}$, with advanced substitution of cerium for strontium, the Madelung energy of the system would increase so that the stability of the perovskite phase might be improved and the symmetry become better, notwithstanding the increase in unit cell volume V.

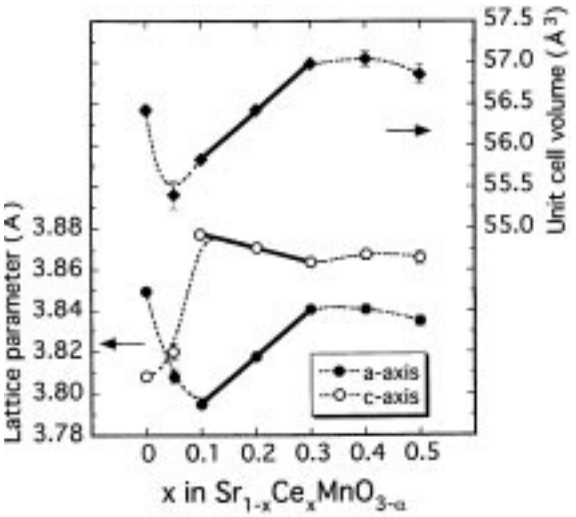

Fig. 3. Lattice parameter and unit cell volume of $Sr_{1-x}Ce_xMnO_{3-\alpha}$ as a function of dopant concentration.

3.2. *Thermal Stability*

Un-doped perovskite $SrMnO_3$ is unstable below 1400°C. Fig. 4(a) shows the X-ray diffraction pattern of $SrMnO_3$ quenched in water from 1500°C. The specimen contained two phases composed of the hexagonal 4L phase and the perovskite phase because of imperfect quenching. After heat treatment at 800°C for 100 h, the $SrMnO_3$ transformed to the hexagonal

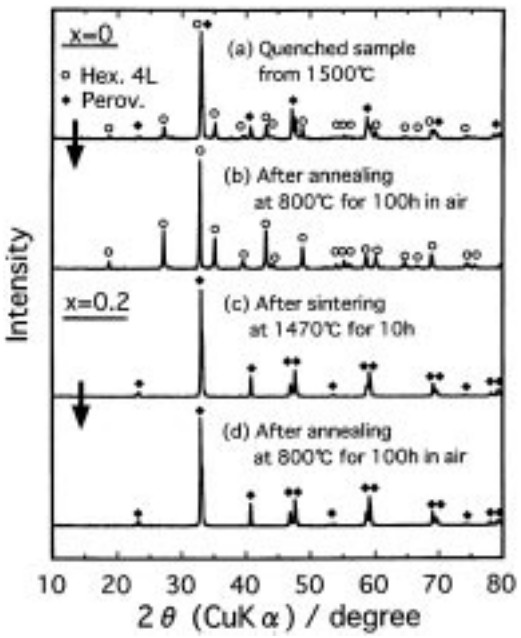

Fig. 4. Thermal stability of $Sr_{1-x}Ce_xMnO_{3-\alpha}$. X-ray diffraction patterns of (a) quenched $SrMnO_3$ from 1500°C, (b) quenched $SrMnO_3$ after annealing at 800°C for 100 h, (c) $Sr_{0.8}Ce_{0.2}MnO_{3-\alpha}$ after sintering at 1470°C for 10 h, (d) sintered $Sr_{0.8}Ce_{0.2}MnO_{3-\alpha}$ after annealing at 800°C for 100 h.

4L single- phase (Fig. 4(b)). This result is in accord with that reported by Negas and Roth [2].

In contrast, $Sr_{0.8}Ce_{0.2}MnO_{3-\alpha}$ had the stable perovskite structure even after heat treatment at 800°C for 100 h. Figs. 4(c) and (d) indicate no change in X-ray diffraction pattern before and after the heat treatment. The stability of $Sr_{0.5}Ce_{0.5}MnO_{3-\alpha}$, which was in the two phase region, was as high as that of $Sr_{0.8}Ce_{0.2}MnO_{3-\alpha}$. In addition to this thermal stability test, DTA of the $Sr_{1-x}Ce_xMnO_{3-\alpha}$ system ($x = 0.2,\ 0.3,\ 0.4$) showed no special peak for transformation up to 1000°C. This might suggest that the increase in the Madelung potential by the substitution of cerium for strontium would also be very effective for thermal stability of the perovskite phase at intermediate temperature.

3.3. Thermal Expansion

Figure 5 shows linear thermal expansion of $Sr_{1-x}Ce_xMnO_{3-\alpha}$ in air up to 1000°C taking 50°C as a standard temperature. A drastic change of thermal expansion, which would indicate a phase transition or transformation, was not observed in the temperature range measured. Hexagonal $SrMnO_3$ had a greater thermal expansion coefficient than that of the perovskite $Sr_{1-x}Ce_xMnO_{3-\alpha}$. According to Negas and Roth, hexagonal $SrMnO_3$ begins to be reduced and to distort its structure in the temperature range of 1035–1400°C as a pre-step for the phase transition to the anion-deficient perovskite structure [2]. Our measurement temperature region is lower than this condition. However, the lattice vibration of the hexagonal $SrMnO_3$ becomes more intense with increasing temperature. This lattice vibration would cause anisotropic thermal expansion, which could not be verified due to polycrystalline nature of the specimen.

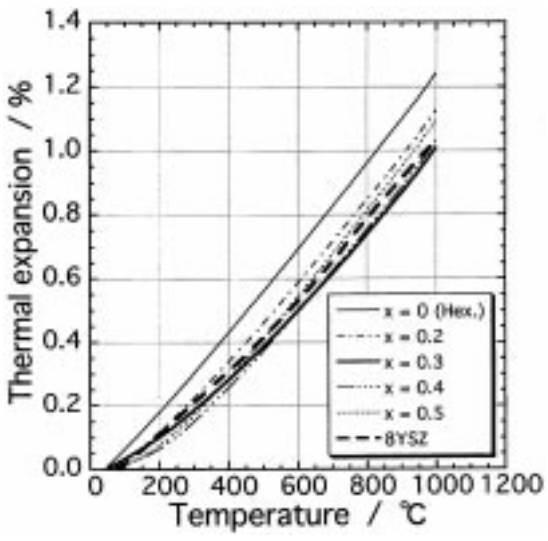

Fig. 5. Linear thermal expansions of $Sr_{1-x}Ce_xMnO_{3-\alpha}$ (50–1000°C, 8YSZ data: [7]).

On the other hand, in case of the perovskite $Sr_{1-x}Ce_xMnO_{3-\alpha}$, the structure was stabilized by substitution of cerium for strontium and the Madelung energy increased. As a result, the lattice vibration is more inactive than that of the hexagonal $SrMnO_3$, and the thermal expansion decreases. The thermal expansion coefficient of $Sr_{0.7}Ce_{0.3}MnO_{3-\alpha}$ was 10.1×10^{-6} cm/cm · K from 50°C to 1000°C, which is fairly close to that of YSZ (about 10.3×10^{-6} cm/cm · K [7]).

In the two phase region ($x \geq 0.4$), where CeO_2 coexists, macroscopic factors, such as grain size, grain shape, grain boundary condition and void distribution become more important for the thermal expansion in addition to microscopic factors, such as crystal structure, interatomic distance, etc.

3.4. Electrical Conductivity

The electrical conductivity of sintered specimens was measured in air from room temperature to 1000°C (Fig. 6). The non-doped hexagonal $SrMnO_3$ showed semiconducting behavior and the conductivity varied from 6.0×10^{-6} S · cm^{-1} to approximately 0.5 S · cm^{-1} in the measurement temperature range. In low temperature region (25–200°C), the conductivity of the specimen was in good agreement with the data which was reported by Lee and Iguchi [8]. In contrast to the hexagonal $SrMnO_3$, Ce doped specimen had the higher conductivity and the behavior was close to semi-metallic. Especially, $Sr_{0.7}Ce_{0.3}MnO_{3-\alpha}$, which had the highest Ce-content in the single phase perovskite, showed the highest conductivity of over 300 S · cm^{-1} in the temperature range of 600–800°C and 60 S · cm^{-1} at room temperature. These values are greater than that of $Ca_{0.9}Ce_{0.1}MnO_{3-a}$ (200 S · cm^{-1} at 700°C) previously reported [1] and that of $La_{0.8}Sr_{0.2}MnO_{3\pm\delta}$ (LSM, 175 S · cm^{-1} at 1000°C) [14] which is being used as a cathode material for SOFC under development. The vast

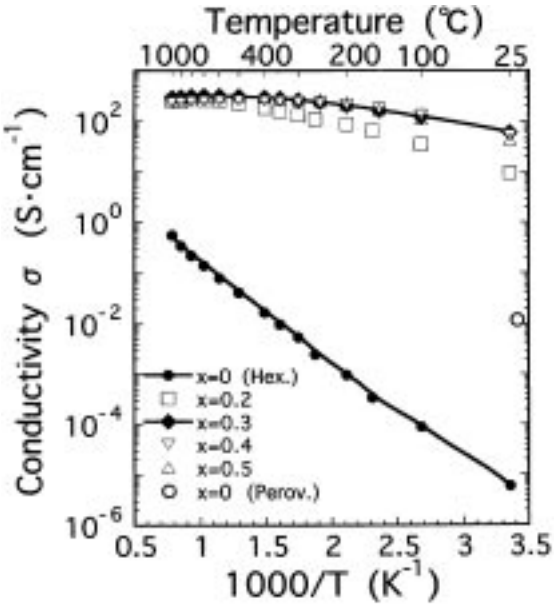

Fig. 6. Conductivity of $Sr_{1-x}Ce_xMnO_{3-\alpha}$ (O: Quenched sample from 1600°C [8]).

difference in conductivities between the hexagonal $SrMnO_3$ and the perovskite $Sr_{1-x}Ce_xMnO_{3-\alpha}$ comes from the difference in crystalline structure and the different manganese valences. The hexagonal structure doesn't have higher symmetry than the perovskite, and the MnO_6 octahedra of the hexagonal share the corners and the faces as shown in Fig. 7 schematically [2,4]. There are two different kinds of Mn-O-Mn angles in the hexagonal crystal, about 180° and 90°, whereas in the perovskite-type, there is only one kind of angle, about 180°. Mn-O-Mn angle affects the gap of the Mn-O band directly. If the Mn-O-Mn angle comes closer to 180°, overlap between oxygen 2p orbital and manganese $3d_{x^2-y^2}$ orbitals becomes

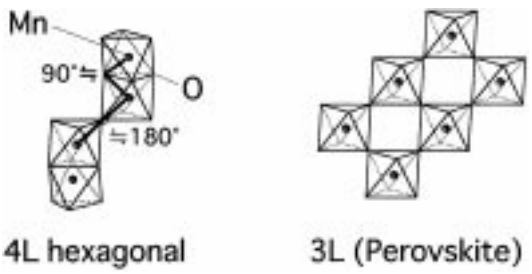

Fig. 7. The projection of MnO_6 octahedra network in hexagonal 4L or perovskite $SrMnO_3$ ([4]).

greater and the Mn-O band gap decreases [8,9]. As a result, $Sr_{1-x}Ce_xMnO_{3-\alpha}$ has a higher conductivity than the hexagonal $SrMnO_3$.

In addition to the good symmetric structure, $Sr_{1-x}Ce_xMnO_{3-\alpha}$ has a high concentration of charge carriers which are induced by a shift of some manganese from $+4$ to $+3$. The quenched perovskite $SrMnO_{3-\alpha}$ was easily reoxidized to cubic perovskite $SrMnO_3$ at low temperature [8]. Although the symmetry of the perovskite $SrMnO_3$ is higher than that of $Sr_{1-x}Ce_xMnO_{3-\alpha}$, the conductivity shows lower values than that of $Sr_{1-x}Ce_xMnO_{3-\alpha}$ (Fig. 6). This fact reflects that the partial substitution of cerium for strontium causes a shift of manganese valence and increases the concentration of charge carriers.

In case of $Sr_{0.7}Ce_{0.3}MnO_{3-\alpha}$, the symmetry and the cerium concentration which caused the change in manganese valence were the highest in the perovskite single phase region, so that the conductivity became the highest in the system. Trofimenko et al. reported the electrical properties of $Sr_{1-x}Ce_xFeO_{3-\alpha}$ and $Sr_{1-x}Ce_xCoO_{3-\alpha}$ system [10,11]. The conductivity of $Sr_{0.7}Ce_{0.3}MnO_{3-\alpha}$ was higher than that of $Sr_{1-x}Ce_xFeO_{3-\alpha}$ ($x = 0.05$, $80\,S \cdot cm^{-1}$ at 500°C) and lower than that of $Sr_{1-x}Ce_xCoO_{3-\alpha}$ ($x = 0.15$, $500\,S \cdot cm^{-1}$ at about 350°C). This tendency would be explained by the differences in the electronic structural factor, and it is similar to other well-known perovskites, e.g. $La_{1-x}Sr_xMO_3$ (M = Mn, Fe, Co), $Pr_{1-x}Sr_xMO_3$ (M = Mn, Co) and so on [12–16].

For each $Sr_{1-x}Ce_xMO_{3-\alpha}$ (M = Mn, Fe, Co), there is a two phase region where perovskite and CeO_2 coexist. In the two phase regions of the $Sr_{1-x}Ce_xFeO_{3-\alpha}$ and $Sr_{1-x}Ce_xCoO_{3-\alpha}$ systems, the conductivity became much lower than that of the perovskite single phase [10,11]. However, in the $Sr_{1-x}Ce_xMnO_{3-\alpha}$ system, the conductivity in the two phase region ($x \geq 0.4$) was not so drastically lowered as those of $Sr_{1-x}Ce_xFeO_{3-\alpha}$ and $Sr_{1-x}Ce_xCoO_{3-\alpha}$.

3.5. *Seebeck Coefficient*

Seebeck coefficients of $Sr_{0.8}Ce_{0.2}MnO_{3-\alpha}$ and $Sr_{0.7}Ce_{0.3}MnO_{3-\alpha}$ in air are given in Fig. 8. In the whole range of temperature examined, the Seebeck coefficients of both specimen were negative, indicating that the charge carriers in $Sr_{0.8}Ce_{0.2}MnO_{3-\alpha}$ and $Sr_{0.7}Ce_{0.3}MnO_{3-\alpha}$ were electrons. This suggests that the concentration of Mn^{4+} is higher than that of Mn^{3+}.

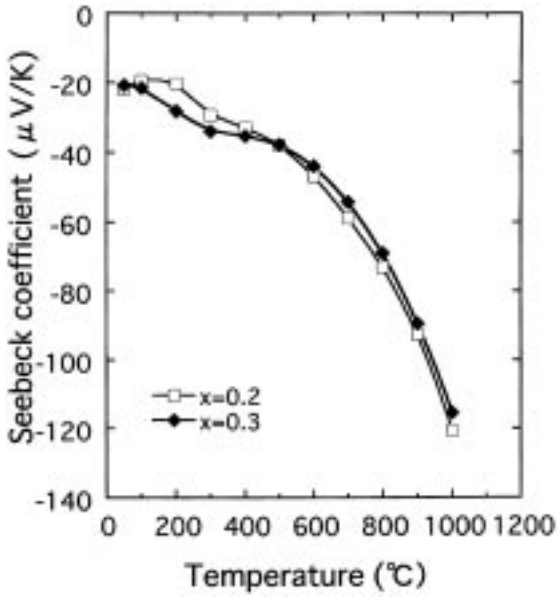

Fig. 8. Seebeck coefficient of $Sr_{1-x}Ce_xMnO_{3-\alpha}$.

The Seebeck coefficient also reflects the fraction of available hopping sites occupied, i.e. concentration of charge carriers. Assuming that spin degeneracy of carriers can be ignored in the system, the fraction of available sites, C, follows Eq. (1) [14,18].

$$C = 1/[1 + \exp(a/86.17)] \quad (1)$$

where a is the absolute value of the Seebeck coefficient in units of mV/K. According to Eq. (1), Fig. 8 shows that C decreases as the temperature increases in the $Sr_{1-x}Ce_xMnO_{3-\alpha}$ system. ($C = 0.44$, at room temperature, $C = 0.21$ at 1000°C in $Sr_{0.7}Ce_{0.3}MnO_{3-\alpha}$). Generally, in the perovskite-type oxides, in which transition metal M takes the mixed valence state, it is known that the M^{+3} ion disproportionates to M^{+2} and M^{+4} and that the disproportionation is thermally excited [12,17,18]. Since the M^{+2} ion does not participate in charge conduction, the available site fraction C decreases as the temperature increases.

In case of the $Sr_{1-x}Ce_xMnO_{3-\alpha}$ system, besides disproportionation of Mn^{3+}, the increase in oxygen vacancies with temperature induces valence variation from Mn^{4+} to Mn^{3+} and the number of available site fraction C will increase. However, this behavior is very minor compared with disproportionation. As a result, the absolute value of the Seebeck coefficient increases with temperature. Inasmuch as the disproportionation and the oxygen reduction don't occur so much at low temperature (under 200°C), the temperature dependence of the Seebeck coefficient is weak as shown in Fig. 8. This inclination agrees with thermal expansion behavior at low temperature (Fig. 5).

In Fig. 8, the temperature dependencies of the Seebeck coefficients of $Sr_{0.8}Ce_{0.2}MnO_{3-\alpha}$ and $Sr_{0.7}Ce_{0.3}MnO_{3-\alpha}$ were almost identical although cerium concentrations were different.

4. Conclusion

We found that $SrMnO_3$ could be stabilized in the perovskite structure even at room temperature by substituting a certain level of cerium for strontium. The stability was so high that the perovskite phase was maintained even after heat treatment at 800°C for 100 h. $Sr_{0.7}Ce_{0.3}MnO_{3-\alpha}$ has the tetragonal crystal structure in which the length of a-axis (3.84 Å) was relatively close to that of the c-axis (3.86 Å), and this phase showed very high conductivity, e.g. $290\,S \cdot cm^{-1}$ at 1000°C and $60\,S \cdot cm^{-1}$ at room temperature. This value was higher than that of $La_{0.8}Sr_{0.2}MnO_{3-\alpha}$. The high conductivity of $Sr_{0.7}Ce_{0.3}MnO_{3-\alpha}$ is explained to result from the highly symmetric structure, as well as high concentration of charge carriers caused by the shift of some of the manganese ions from $+4$ to $+3$.

References

1. H. Iwahara, T. Esaka, and H. Hamajima, *DENKI KAGAKU*, **57**, 591 (1989).
2. T. Negas and R.S. Roth, *J. Solid State Chem.*, **1**, 409 (1970).
3. L. Katz and R. Ward, *Inorg. Chem.*, **3**, 205 (1964).
4. J.M. Longo and J.A. Kafalas, *J. Solid State Chem.*, **1**, 103 (1969).
5. R.D. Shannon, *Acta Crystallogr.*, **A32**, 751 (1976).
6. W.A. Harrison, *Electronic Structure and the Properties of Solids: The Physics of the Chemical Band* (W.H. Freeman and Company, 1980).
7. The Central Research Institute of Electric Power Industry (CRIEPI), Japan, Yokosuka Research Lab. Rep. No. W97003 (1998).
8. K.J. Lee and E. Iguchi, *J. Solid State Chem.*, **114**, 242 (1995).
9. J.B. Torrance, P. Lacorre, A.I. Nazzal, E.J. Ansaldo, and Ch. Niedermayer, *Phys. Rev.*, **B45**, 8209 (1992).
10. N.E. Trofimenko, H. Ullmann, J. Paulsen, and R. Müller, *Solid State Ionics*, **99**, 201 (1997).
11. N.E. Trofimenko, J. Paulsen, H. Ullmann, and R. Müller, *Solid State Ionics*, **100**, 183 (1997).

12. G.Ch. Kostogloudis, N. Vasilakos, and Ch. Ftikos, *Solid State Ionics*, **106**, 207 (1998).
13. T. Ishihara, T. Kudo, H. Matsuda, and Y. Takita, *J. Electrochem. Soc*., **142**, 1519 (1995).
14. J.H. Kuo, H.U. Anderson, and D.M. Sparlin, *J. Solid State Chem*., **87**, 55 (1990).
15. A. Mineshige, M. Inaba, T. Yao, Z. Ogumi, K. Kikuchi, and M. Kawase, *J. Solid State Chem*., **121**, 423 (1996).
16. J. Mizusaki, T. Sasamoto, W.R. Cannon, and H.K. Bowen, *J. Am. Ceram. Soc*., **66**, 247 (1983).
17. J. Mizusaki, H. Tagawa, K. Naraya, and T. Sasamoto, *J. Solid State Ionics*, **49**, 111 (1991).
18. J.W. Stevenson, M.M. Nasrallah, and H.U. Anderson, *J. Solid State Chem*., **102**, 175 (1993).